

Small-angle scattering from the Cantor surface fractal on the plane and the Koch snowflake

A. Yu. Cherny,^{1,2,*} E. M. Anitas,^{1,3} V. A. Osipov,¹ and A. I. Kuklin^{1,4}

¹Joint Institute for Nuclear Research, Dubna 141980, Russian Federation

²Center for Theoretical Physics of Complex Systems, Institute for Basic Science (IBS), Daejeon 34051, Republic of Korea

³Horia Hulubei National Institute of Physics and Nuclear Engineering, RO-077125 Bucharest-Magurele, Romania

⁴Laboratory for Advanced Studies of Membrane Proteins,

Moscow Institute of Physics and Technology, Dolgoprudny, Russian Federation

(Dated: October 3, 2016)

The small-angle scattering (SAS) from the Cantor surface fractal on the plane and Koch snowflake is considered. The surface fractals can be represented as a sum of surface mass fractals for arbitrary fractal iteration. It is shown that for the Cantor fractal, one can neglect with a good accuracy the correlations between the mass fractal amplitudes, while for the Koch snowflake, these correlations are important. The developed model explains the decay of the scattering intensity $I(q) \sim q^{D_s-4}$ with $1 < D_s < 2$ being the fractal dimension of the perimeter. The curve $I(q)q^{4-D_s}$ is found to be log-periodic in the fractal region with the period equal to the scaling factor of the fractal. The log-periodicity arises from the self-similarity of sizes of basic structural units rather than from correlations between their distances. A recurrence relation is obtained for the radius of gyration of Koch snowflake. The present analysis enables us to obtain additional information from SAS data, such as the edges of the fractal regions, the fractal iteration number and the scaling factor.

PACS numbers: 05.45.Df, 61.43.Hv, 61.05.fg, 61.05.cf

I. INTRODUCTION

The small-angle scattering (SAS) of waves (e.g. neutrons, X-rays, light) [1–4] is an important non-destructive method in determining the structural properties (internal structure, shape, size, positional correlations, average spatial arrangement, molecular weight, fractal dimension) of fractal and/or disordered systems (polymers, complex fluids, aggregates, colloids) at nano and microscales [5–9]. In particular, by using the framework provided by deterministic (exact self-similar) fractals, it has been shown more recently that the range of structural properties which can be extracted can be significantly extended to include additional information, such as the scaling factor, iteration number or the number of particles constituting the fractal [10, 11]. These information are usually extracted from a double logarithmic plot of the normalized elastic cross section per unit volume of the sample (scattering intensity) $I(q) \equiv (1/V')d\sigma/d\Omega$ plotted versus the scattering wave vector $q = (4\pi/\lambda)\sin\theta$ (θ is half the scattering angle and λ is the wavelength of the incident radiation) which describes, through a Fourier transform, the spatial density-density correlations of the system. Therefore, the information obtained by using SAS coupled with the theoretical framework provided by the fractal geometry [12, 13] allows us to have a better understanding of the structural properties of such systems.

An important characteristic, which makes SAS a unique tool in analyzing experimental data from fractal systems is the possibility to differentiate between “mass” and “surface” fractals [5, 7]. The difference arise from the value of the scattering exponent τ of the simple power-law SAS intensity:

$$I(q) \propto q^{-\tau}, \quad (1)$$

where the scattering exponent can be written in the following way

$$\tau = \begin{cases} D_m, & \text{for mass fractals,} \\ 2d - D_s, & \text{for surface fractals.} \end{cases} \quad (2)$$

Here, d is the topological dimension of the space into which the fractal is embedded, D_m is the mass fractal dimension satisfying the condition $0 < D_m < d$, and D_s is the surface fractal dimension, satisfying $d - 1 < D_s < d$. For three-dimensional space ($d = 3$), this leads to a simple interpretation of SAS experimental data: if the power-law exponent $\tau < 3$, the measured sample is a mass fractal, while if $3 < \tau < 4$ then the sample is a surface fractal. One can adopt a simple descriptive definition of the Hausdorff dimension D of a set as the exponent in the relation $N \propto (1/a)^D$ for $a \rightarrow 0$, where N is the minimum number of open sets of diameter a needed to cover the set. For a “usual” globular object like ball, the Hausdorff dimensions of volume and surface are equal to 3 and 2, respectively.

Sometimes a succession of simple power-law decays with different exponents can be observed in SAS data, which can be explained by the presence of a fractal structures at different scales in monophasic [9, 14] and multiphase [15] systems.

Recently, it has been shown that the 3D Cantor-like surface fractal at m -th iteration can be represented as a sum of Cantor mass fractals at iterations from zero to m , and it has been suggested [16] that, in general, *any surface fractal can be represented as a sum of mass fractals*. This statement should be used with minor reservations [16]. First, adding additional measure to a fractal support amounts to subtracting the same measure from the complement set of the fractal. Then the fractal support of the complementary set can be constructed by a subsequent *subtraction* of mass-fractal iterations. This does not play a role in SAS scattering, since two complementary sets give the same diffraction pattern (Babinet’s principle). Second, the notion of mass fractal should be used here

* e-mail: cherny@theor.jinr.ru

with caution, because the limit of *infinite* iterations might not exist in the rigorous mathematical sense. However, once a surface fractal is realized in real material, the fractal iterations of composing mass fractals have to be *finite* and always exist, which makes this mathematical problem not relevant from a physical point of view. For a finite iteration of mass fractal, all the scaling fractal properties are confined to a finite range in real space, whether the limit of infinite iterations exists or not. The bigger the iteration number, the longer the fractal range in real space, but the fractal scaling properties within this range would be the same as if the limit of infinite iterations existed.

It has been shown [16] that the “rough structure” of the scattering intensity can be explained in terms of power-law distribution of sizes of objects composing the fractal. The power-law decay $I(q) \propto q^{D_s-6}$ is realized as a non-coherent sum of scattering amplitudes of 3D objects composing the fractal and obeying a power-law distribution $dN(r) \propto r^\tau dr$, with $D_s = \tau - 1$. We mean by rough structure that not all minima and maxima superimposed on the power-law decay appear within this approximation.

Here, we apply the above findings to the well-known 2D Koch snowflake and Cantor surface fractals. The SAS intensity is calculated in momentum space and analyzed. We suggest a new algorithm for constructing the Koch snowflake and show that the curve $I(q)q^{4-D_s}$ with $1 < D_s < 2$, is log-periodic with the period equal to the scaling factor of the fractal. A recurrence relation is obtained for the radius of gyration of Koch snowflake. The present analysis might be useful for obtaining structural information (overall dimension of the fractal, size of the smallest structural unit composing the fractal, the fractal iteration number, and the scaling factor) from various artificially prepared nano and micro systems, such as for the recently obtained molecular Sierpinski hexagonal gasket incorporating the Star of David and the Koch snowflake motifs [17] or the three-dimensional analog of the Koch snowflake [18].

II. THEORETICAL BACKGROUND

In a very good approximation, the differential cross section of a sample exposed to a beam of neutrons, X-rays or light is given by [1, 2] $d\sigma/d\Omega = |A'(\mathbf{q})|^2$, where $A'(\mathbf{q}) \equiv \int_{V'} \rho_s(\mathbf{r}) e^{i\mathbf{q}\cdot\mathbf{r}} d^3r$ is the total scattering amplitude, V' is the total volume irradiated by the incident beam, and the scattering length density $\rho_s(\mathbf{r})$ is defined with the help of Dirac's δ function: $\rho_s(\mathbf{r}) = \sum_j b_j \delta(\mathbf{r} - \mathbf{r}_j)$. Here, \mathbf{r}_j are the positions of microscopic objects like atoms or nuclei.

Let us consider a sample consisting of rigid *macroscopic* objects of the density ρ_m , which are immersed into a solid matrix of density ρ_p , and suppose that spatial positions and orientations are uncorrelated (this assumes that the concentration of the objects in the solid matrix is low enough). Then the scattering intensity (differential cross section per unit volume of the sample) can be written as

$$I(q) \equiv \frac{1}{V'} \frac{d\sigma}{d\Omega} = n |\Delta\rho|^2 V^2 \langle |F(\mathbf{q})|^2 \rangle, \quad (3)$$

where n is the concentration of the macroscopic objects in the irradiated volume, $\Delta\rho = \rho_m - \rho_p$ is the scattering contrast, V is the volume of each object and $F(\mathbf{q})$ is the normalized scattering amplitude (form factor) of the object

$$F(\mathbf{q}) = \frac{1}{V} \int_V e^{-i\mathbf{q}\cdot\mathbf{r}} d\mathbf{r}, \quad (4)$$

obeying the condition $F(0) = 1$. Here, the symbol $\langle \dots \rangle$ stands for the ensemble averaging over all orientations of the objects. If the probability of any orientation is the same, then it can be calculated by integrating over all directions of the scattering vector \mathbf{q} [19].

It is easy to derive a few useful properties of the form factor (4), which are valid for a particle of arbitrary shape.

i) Scaling: if we scale all the lengths of particle as $l \rightarrow \beta l$ then $F(\mathbf{q}) \rightarrow F(\beta\mathbf{q})$.

ii) Translation: if the particle is translated $\mathbf{r} \rightarrow \mathbf{r} + \mathbf{a}$ then $F(\mathbf{q}) \rightarrow F(\mathbf{q}) \exp(-i\mathbf{q} \cdot \mathbf{a})$.

iii) Rotation: if the particle is rotated with an orthogonal matrix $\mathbf{r} \rightarrow \hat{O}\mathbf{r}$ then $F(\mathbf{q}) \rightarrow F(\hat{O}^T\mathbf{q})$. Recall that the inverse orthogonal matrix is equal to the transposed matrix $\hat{O}^{-1} = \hat{O}^T$, where $(\hat{O}^T)_{ij} = \hat{O}_{ji}$.

iv) Additivity of the nonnormalized scattering amplitude: if a particle consists of two not overlapping subsets I and II, then $F(\mathbf{q}) = (V_I F_I(\mathbf{q}) + V_{II} F_{II}(\mathbf{q})) / (V_I + V_{II})$.

The average over all directions of the scattering vector \mathbf{q} in Eq. (3) is analogous to diffraction with an entirely uncollimated beam in optics [11]. This results in strong spatial incoherence: for the subsets I and II, the correlator $\langle F_I(\mathbf{q}) F_{II}(\mathbf{q}) \rangle$ decays when $q \gg 2\pi/r$, where r is of order of the distance between their centers [11]. This indicates the border between the coherent regime (where the scattering amplitudes $V_I F_I$ and $V_{II} F_{II}$ should be added) and incoherent regime (where the scattering intensities $\langle |V_I F_I|^2 \rangle$ and $\langle |V_{II} F_{II}|^2 \rangle$ should be added).

For a “primary” globular object like a ball or cube of total size l , the intensity $\langle |F(\mathbf{q})|^2 \rangle$ is of order one in the Guinier range $q \lesssim 2\pi/l$ and decays as $1/q^4$ in the Porod range $q \gtrsim 2\pi/l$ [1].

Almost all scattering properties of a complex object can be understood by means of the above simple properties of composing “primary” objects and transitions from coherent to incoherent scattering regimes. Below we outline some basic properties of mass and surface fractals.

For a mass fractal of the total length L , composed of p small “primary” structural units of size l separated by distances d ($l \lesssim d \lesssim L$), the normalized form factor can be estimated qualitatively by the formula

$$\langle |F_m(\mathbf{q})|^2 \rangle \simeq \begin{cases} 1, & q \lesssim 2\pi/L, \\ (qL/2\pi)^{-D_m}, & 2\pi/L \lesssim q \lesssim 2\pi/d, \\ (L/d)^{-D_m}, & 2\pi/d \lesssim q \lesssim 2\pi/l, \\ (L/d)^{-D_m} (ql/2\pi)^{-4}, & q \gtrsim 2\pi/l. \end{cases} \quad (5)$$

Here p is of the order of $(L/d)^{D_m}$ in accordance with the definition of the fractal dimension.

For a surface fractal composed of “primary” units, the distances between which are assumed to be spatially *uncorrelated*, the qualitative formula takes the form

$$\langle |F_s(\mathbf{q})|^2 \rangle \simeq \begin{cases} 1, & q \lesssim 2\pi/L_0, \\ (qL_0/2\pi)^{D_s-6}, & 2\pi/L \lesssim q \lesssim 2\pi/l, \\ (L_0/l)^{D_s-6} (ql/2\pi)^{-4}, & q \gtrsim 2\pi/l, \end{cases} \quad (6)$$

and in this case L_0 and l is of the order of the largest and smallest sizes of the units, respectively. Equation (5) explicitly shows that the SAS intensity of mass fractal is characterized by the four main regions: Guinier at $q \lesssim 2\pi/L$, fractal at $2\pi/L \lesssim q \lesssim 2\pi/d$, a plateau at $2\pi/d \lesssim q \lesssim 2\pi/l$, and Porod regime at $q \gtrsim 2\pi/l$.

We make a few remarks here. First, the intensity in the Guinier range is actually parabolic: $I(q) \simeq I(0)(1 - R_g^2 q^2/3)$, where R_g is the radius of gyration. This parabolic behavior of the intensity is ignored in the above estimations for the sake of simplicity. Second, the *mass* fractal region appears due to *spatial correlation* of the composing units [10, 11], while the *surface* fractal region appears due to the *power-law polydispersity* of their sizes [16]. For this reason, the fractal region of the mass fractal is determined by the maximal and minimal distances between the centers of the structural units, while the fractal region of the surface fractal is determined by the largest and smallest radii present in the fractal. Third, the plateau at $2\pi/d \lesssim q \lesssim 2\pi/l$ in the scattering intensity of the mass fractal can be considered as a Guinier region for the primary unit (which are of the same size l), because the spatial correlations between different units are not important here anymore.

At n -th iteration, the normalized scattering amplitude for a mass fractal is

$$F_n^{(m)}(\mathbf{q}) = F_0(\beta_s^n q r_0) G_1(\mathbf{q}) G_1(\beta_s \mathbf{q}) \cdots G_1(\beta_s^{n-1} \mathbf{q}), \quad (7)$$

where $F_0(q)$ is the form factor of the basic fractal unit, $G_1(\mathbf{q})$ is the generative function depending on the relative positions of the fractal units inside the fractal, and β_s is the scaling factor of the fractal.

Thus, since the surface fractal is the sum of mass Cantor fractals at various iterations, we shall add the amplitudes of the mass fractal iterations, and normalize the result to one at $q = 0$. Then, for a 3D Cantor-like surface fractal we have [16, 20]

$$F_m^{(s)}(\mathbf{q}) = \frac{1 - k\beta_s^3}{1 - (k\beta_s^3)^{(m+1)}} \sum_{n=0}^m (k\beta_s^3)^n F_n^{(m)}(\mathbf{q}), \quad (8)$$

where k is the number of balls of radius $r_1 = \beta_s r_0$ which replace the ball of radius r_0 at zero-th iteration (initiator). Then, the final expression for the scattering intensity is given by (see Eq. 3)

$$I_m^{(s)}(q) = I_m^{(s)}(0) \left\langle |F_m^{(s)}(\mathbf{q})|^2 \right\rangle, \quad (9)$$

with $I_m^{(s)}(0) = n |\Delta\rho|^2 V_m^2$, where V_m is the total volume of surface fractal at m -th iteration.

In two dimensional space, the scattering intensity $I(q)$ of a set is calculated by means of averaging the squared scattering amplitude $S^2 \langle |F(\mathbf{q})|^2 \rangle$ with respect to the polar angle in the plane, where S is the area of the set. The normalized amplitude (4) is calculated by integration in the plane: $F(\mathbf{q}) = \int_S e^{-i\mathbf{q}\cdot\mathbf{r}} d\mathbf{r} / S$. The intensity decays for large scattering vectors as $I(q) \propto q^{4-D_s}$ with $1 < D_s < 2$, see Eq. (2). Here the “surface” dimension D_s is nothing else but the Hausdorff dimension of perimeter bounding the fractal support in the plane. For this reason, it would be more natural to talk about a “perimeter” fractal in the plane, but we use, nevertheless, the well-known “three-dimensional” terminology [16] and adopt the notation D_s . The perimeter of a “usual” object, like disk or rectangle, is a one-dimensional line ($D_s = 1$).

III. CANTOR-LIKE SURFACE FRACTAL

A. Construction and properties

The construction process of 2D Cantor-like surface fractal is similar to that of 3D version [16] in the sense that one follows a “top-down” approach in which an initial structure is repeatedly divided (by a single scaling factor) into a set of smaller structures of the same type according to a given rule which is kept the same from one iteration to the next one.

The Cantor surface fractal is constructed as a sum of mass generalized Cantor fractals (GCF), which are suggested and discussed in detail in Refs. [10, 11]. The GCF is also called Cantor dust. Let us recall the construction algorithm for the GCF. We start with a square of edge L and choose a Cartesian system of coordinates with the origin in the square center, and the axes parallel to the cube edges. The zeroth iteration (called initiator) is a disk of radius r_0 in the origin. The iteration rule (generator) is to replace the disk with k smaller disks ($k = 4$) of radius $r_1 = \beta_s r_0$, where the parameter β_s , called scaling factor, obeys the condition $0 < \beta_s < 1/2$. The centers of the four disks of radius r_1 are shifted from the origin by the four vectors

$$\mathbf{a}_j = \frac{1 - \beta_s}{2} L \{ \pm 1, \pm 1 \} \quad (10)$$

with all the combinations of the signs. The next iterations are obtained by performing an analogous operation to each of k balls of radius r_1 , and so on (see Fig. 1). The fractal dimension of the Cantor dust (mass Cantor fractal) is given by [10]

$$D_m = -\ln k / \ln \beta_s \quad (11)$$

with $k = 4$ for the Cantor dust in two dimensions. It lies within $0 < D_m < 2$.

The m -th iteration of the Cantor-like surface fractal is built as a *sum* of the Cantor dusts of iterations from zero to m , see Fig. 1. In order to avoid the overlapping between the different iterations of the Cantor dust, the initial radius should be restricted: $r_0 \leq L(1 - 2\beta_s)/2$. Thus, the largest size contained in Eq. (6) is equal to $L_0 = 2r_0$. By the construction, the initial length L is nothing else but the size of the surface

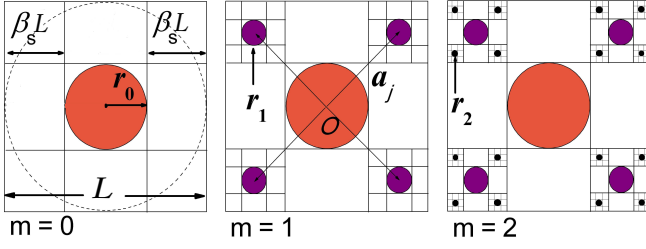


FIG. 1. (Color online) Construction of Cantor-like surface fractals at $m = 2$ as a sum of Cantor mass fractals at: $m = 0$ (disk of radius r_0 ; orange), $m = 1$ (disks of radii $r_1 = r_0\beta_s$; violet) and $m = 2$ (disks of radii $r_2 = r_0\beta_s^2$; black). The vectors \mathbf{a}_j , $j = 1, 2, 3, 4$ connect the center of disk of radius r_0 with the centers of disks of radii r_1 . The components of these vectors are $\pm(1 - \beta_s)L/2$.

fractal if m is big enough. The main difference between the Cantor mass and surface fractals is that, at a given iteration, the mass fractal consists of subunits with the same size, while the surface fractal consists of subunits with different sizes. As we shall see below, this property is responsible for the scattering behavior $I(q) \propto q^{D_s-4}$. The difference is apparent from Fig. 1.

At the m -th iteration, the two-dimensional Cantor-like surface fractal is composed of $N_m = 1 + k + k^2 + \dots + k^m$ balls

$$N_m = (k^{m+1} - 1)/(k - 1) \quad (12)$$

(with $k = 4$), whose radii and surface areas are distributed in the following way. One disk of radius r_0 has area πr_0^2 , k disks of radius $r_1 = \beta_s r_0$ have the area $k\pi r_1^2$, k^2 disks of radius $r_2 = \beta_s^2 r_0$ have the area $k^2\pi r_2^2$, and so on. Then, the total area of surface fractal at m -th iteration is given by

$$S_m = S_0 \frac{1 - (k\beta_s^2)^{m+1}}{1 - k\beta_s^2} \quad (13)$$

with the volume of zero iteration $S_0 = \pi r_0^2$. Because of the inequality $k\beta_s^2 < 1$, the total area (13) is finite in the limit $m \rightarrow \infty$, and then the Hausdorff dimension of the fractal surface is equal to 2.

The contribution of the initiator ($m = 0$) to the Hausdorff dimension of the total perimeter of the Cantor-like fractal is obviously equal to 1, which yields the lower limit for the surface dimension, while the contribution of the m -th mass iteration for $m \rightarrow \infty$ is given by the fractal dimension (11). Then we arrive at the Hausdorff (fractal) dimension of the total perimeter of the Cantor-like fractal

$$D_s = \begin{cases} 1, & \text{for } 0 < \beta_s \leq 1/k, \\ -\ln k / \ln \beta_s, & \text{for } 1/k \leq \beta_s < 1/2. \end{cases} \quad (14)$$

The threshold value $\beta_s = 1/k$ corresponds to $D_m = 1$ in Eq. (11), which yields $\beta_s = 0.25$ for $k = 4$. When the scaling factor β_s smaller than this value, the total surface of the fractal is finite even in the limit $m \rightarrow \infty$. As expected [5, 6, 8], the surface Hausdorff dimension satisfies the condition $1 < D_s < 2$.

B. Fractal form factor

In two dimensions, the number of disks in the first iteration of the mass fractal is $k = 4$ and their radius is $r_1 = \beta_s r_0$. The form factor of a disk of unit radius is given by [1]

$$F_0(z) = 2J_1(z)/z, \quad (15)$$

where $J_1(z)$ is the Bessel function of the first kind of order one. The generative function is $G_1(\mathbf{q}) \equiv \cos(uq_x)\cos(uq_y)$, where $u \equiv L(1 - \beta_s)/2$.

By neglecting the correlations between the amplitudes of different mass fractal iterations (that is $\langle F_n^{(\text{mf})}(\mathbf{q})F_j^{(\text{mf})}(\mathbf{q}) \rangle \simeq 0$ for $n \neq j$) when $q \gtrsim 2\pi/r_{nj}$ with r_{nj} being a typical distance between balls in the n th and j th mass fractal iterations, and using Eq. (9), the scattering takes the form [16]

$$\begin{aligned} I_m^{(\text{sf})}(q)/I_m^{(\text{sf})}(0) &= \langle |F_m^{(\text{sf})}(\mathbf{q})|^2 \rangle \\ &\simeq \frac{(1 - k\beta_s^2)^2}{(1 - (k\beta_s^2)^{m+1})^2} \sum_{n=0}^m (k\beta_s^2)^{2n} \langle |F_n^{(\text{mf})}(\mathbf{q})|^2 \rangle, \end{aligned} \quad (16)$$

Following similar arguments as in Ref. [16] we can rewrite the incoherent sum of scattering intensities of disks as:

$$I^{(\text{s})}(q) \simeq I_0(q) + \beta_s^{4-D_s} I_0(\beta_s q) + (\beta_s^{4-D_s})^2 I_0(\beta_s^2 q) + \dots, \quad (17)$$

where $I_0(q)$ is the scattering intensity of the central scattering disk.

The figure 2 shows that the scattering intensity of a surface fractal is realized approximately as a *non-coherent sum* of intensities of a system of disks. One can see that in the fractal region $\pi/r_0 \lesssim q \lesssim \pi/r_m$, we have a good coincidence between exact formula (9), the approximation (16) neglecting the correlations between mass fractal amplitudes, and completely incoherent sum of intensities of the disks (17), which are discussed in detail in Ref. [16]. The latter approximation is given by Eq. (17) but with $I_0(q) \equiv n|\Delta\rho|^2\pi^2 r_0^4 F_0^2(qr_0)$ and the exponent $4 - \beta_s$. The different curves correspond to different sizes of the initial disk radius r_0 . In both cases, as expected, we can observe the presence of the four main regions of scattering intensities: Guinier, intermediate, fractal, and Porod. In the fractal region, the scattering intensity is approximated well by the non-coherent sum of intensities of all disks. The higher the ratio L/r_0 is, the better the approximation (17) works [16]. Thus, the correlations between spatial positions of the disks can play a role, but they lead only to additional oscillations, while the value of the scattering exponent is preserved, as one can see from Fig. 2. Note that the oscillations would be smeared and not visible at all in practical experimental measurements.

IV. KOCH SNOWFLAKES: CONSTRUCTION AND SCATTERING PROPERTIES

The Koch snowflake (KS) is a two-dimensional surface fractal, which can be constructed as a sum of mass fractals

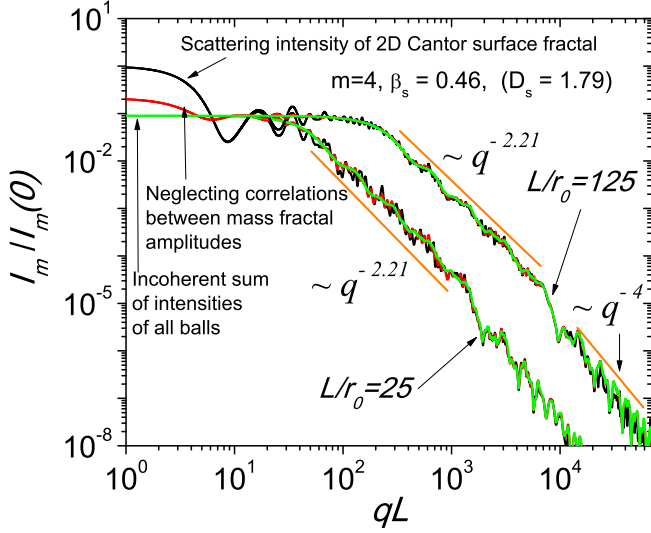


FIG. 2. (Color online) Scattering intensities from two-dimensional Cantor fractals. Note that the condition $L/r_0 \geq 2/(1 - 2\beta_s)$ guarantees the absence of overlapping between the structural units of the Cantor-like surface fractal. One can observe a good agreement between the exact formula, the approximation neglecting the correlations between the mass fractal amplitudes, and completely incoherent sum of intensities of the disks composing the fractal.

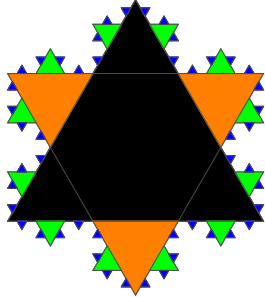


FIG. 3. (Color online) Koch snowflake as a sum of various iterations of mass fractals shown in different colors. The second iteration of Koch snowflake is shown, see Fig. 4.

composed of triangles, see Fig. 3. We start from an initial equilateral triangle (zeroth mass fractal iteration) with edge a and area $S^T = \sqrt{3}a^2/4$. Then each edge is divided into three segments of equal length $a/3$, and an outward equilateral triangle is added with the base coinciding with the center segment. Then the operation is applied repeatedly to each line segment. After m th iterations, the total number of equal edges of length $a_m = a/3^m$ is equal to $3 \cdot 4^m$. Therefore, the Hausdorff dimension of the perimeter is easily calculated as $D_s = \lim_{m \rightarrow \infty} \log(3 \cdot 4^m) / \log(a/a_m) = \log 4 / \log 3 \simeq 1.26$, and thus we have $D_s > 1$.

The n th mass fractal iteration consists of triangles of equal sizes with the edge $a_n = a/3^n$, and their number is equal to $N_n = 3 \cdot 4^{n-1}$ for $n = 1, 2, \dots$. Note that the dimensions of the *mass fractal* and the *perimeter* coincide and equal

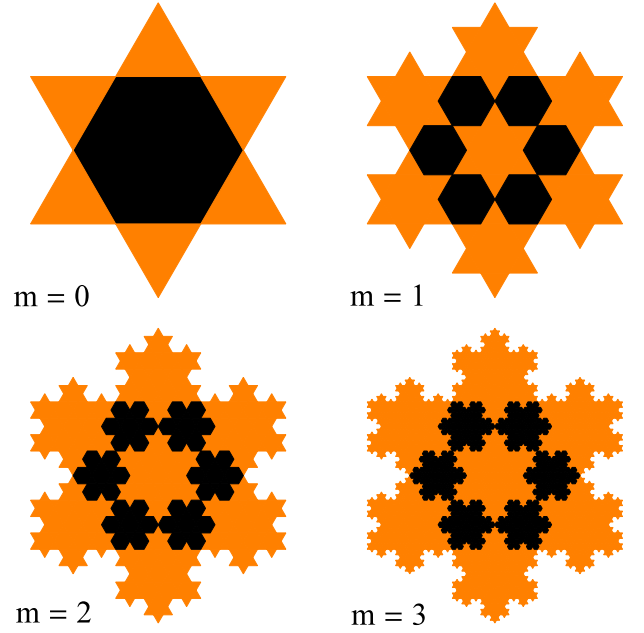


FIG. 4. (Color online) A construction algorithm of the Koch snowflake. The generator ($m = 0$) is built from six triangles (orange) and one hexagon (black). The first iteration is obtained with six hexagons (black) and seven zeroth iterations (orange), scaled with factor $1/3$. For constructing the second iterations, we take the first iteration ($m = 1$) and subtract the six outside zeroth iterations, thus obtaining a “modified hexagon”. The second iteration ($m = 2$) is composed of six “modified hexagons” (black) and seven first iterations (orange), scaled with factor $1/3$. The third iteration is constructed in the same manner.

$D_s = \log 4 / \log 3$. The area of the n th mass fractal iteration is $N_n S^T / 3^{2n}$.

Now it is more convenient to consider the star of David as the initiator KS (the zeroth iteration). Then the total area of KS at the m th iteration is given by

$$S_m = S^T + \sum_{n=1}^{m+1} \frac{S^T}{3^{2n}} N_n = \frac{4S^T}{5} \left(2 - \frac{1}{3} \frac{4^m}{9^m} \right). \quad (18)$$

The area S^{KS} of the ideal KS is obtained from this equation in the limit $m \rightarrow \infty$, which leads to $S^{KS} = 8S^T/5 = 2\sqrt{3}a^2/5$.

The standard algorithm of constructing KS, described above, is not convenient for obtaining the KS scattering amplitude, because it is not simple technically to calculate analytically the positions of the triangles for arbitrary iteration. For this reason, we adopt here a slightly modified algorithm of the paper [21], see Fig. 4. With this algorithm, the recurrence formula for the scattering amplitude $A_m(\mathbf{q}) \equiv S_m F_m(\mathbf{q})$ of the m th iteration of KS can be written down by using the properties of the scattering amplitudes discussed in Sec. II.

$$A_m(\mathbf{q}) = 6G_2(\mathbf{q})[\beta_s^2 A_{m-1}(\beta_s \mathbf{q}) - 6G_1(\beta_s \mathbf{q})\beta_s^4 A_{m-2}(\beta_s^2 \mathbf{q})] + \beta_s^2 A_{m-1}(\beta_s \mathbf{q})[1 + 6G_1(\mathbf{q})] \quad (19)$$

where the scaling factor takes the value $\beta_s = 1/3$, and $G_1(\mathbf{q}) = \frac{1}{6} \sum_{j=0}^5 e^{-i\mathbf{q} \cdot \mathbf{c}_j}$, $G_2(\mathbf{q}) = \frac{1}{6} \sum_{j=0}^5 e^{-i\mathbf{q} \cdot \mathbf{b}_j}$ with

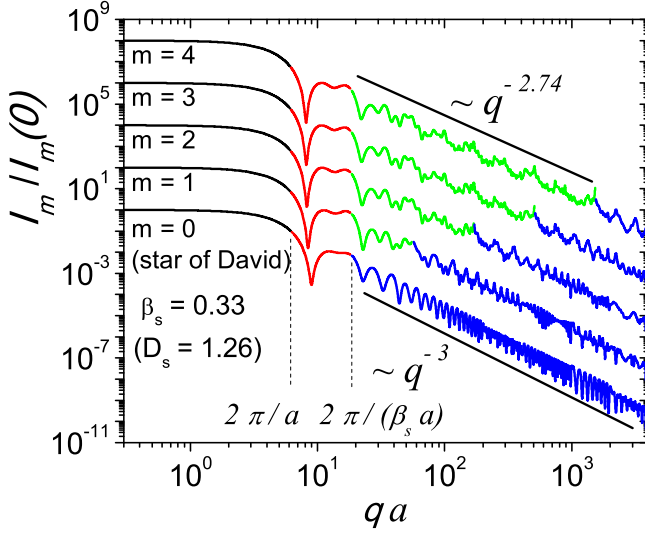


FIG. 5. (Color online) Scattering intensity for the first four iterations of the monodisperse Koch snowflake. Scattering curve for the m th iteration is scaled up for clarity by the factor 10^{2m} . The Guinier, intermediate, fractal, and Porod regions are shown in black, red, green, and blue, respectively.

the translation vectors $\mathbf{b}_j = \frac{2a}{3\sqrt{3}}\{\cos(\pi j/3), \sin(\pi j/3)\}$ and $\mathbf{c}_j = \frac{2a}{9}\{\cos(\pi(j+1/2)/3), \sin(\pi(j+1/2)/3)\}$.

Equation (19) allows us to obtain the nonnormalized scattering amplitude of KS for arbitrary iteration provided the amplitudes of the zeroth and first iterations are known. They can be calculated from the scattering amplitudes of triangles as discussed in Appendix A. The scattering intensity is proportional to the squared amplitude averaged with respect to the polar angle: $I_m(q) \sim \langle |A_m(q)|^2 \rangle$.

Equation (19) can be used to derive the recurrence relations for the area and gyration radius of KS. Indeed, taking this equation at $q = 0$, we have $A_m(0) = S_m$, and $G_1(0) = G_2(0) = 1$. Substituting $\beta_s = 1/3$ yields the recurrence relation for the area $S_m = (13S_{m-1} - 4S_{m-2})/9$, which is consistent well with the explicit formula (18).

The radius of gyration R_m of the m th iteration of KS is determined from the expansion of scattering intensity $I(q) = I(0)(1 - q^2 R_g^2/2 + \dots)$ for $q \rightarrow 0$ at $d = 2$ [2]. Thus, we obtain $I_m(q)/I_m(0) = \langle |A_m(q)|^2 \rangle/S_m^2 = (1 - q^2 R_m^2/2 + \dots)$. If a structure has a rotational symmetry of order $n \geq 3$ with respect to the center-of-mass, then the scattering amplitude is rotationally symmetric at small q up to quadratic terms. KS is invariant under rotation through the angle $\pi/3$ about the center, which implies that the rotational symmetry has the order $n = 6$. This gives us $A_m(q) = S_m(1 - q^2 R_m^2/4 + \dots)$. Substituting this relation and the expansions for $G_1(q) = 1 - a^2 q^2/81 + \dots$ and $G_2(q) = 1 - a^2 q^2/27 + \dots$ into

Eq. (19) yields

$$R_m^2 = \frac{351R_{m-1}^2 S_{m-1} - 12R_{m-2}^2 S_{m-2} + 32a^2(9S_{m-1} - 2S_{m-2})}{2187S_m} \quad (20)$$

The radii of gyration for the first two iterations can be calculated straightforwardly: $R_0^2 = 11a^2/108$ (star of David) and $R_1^2 = 223a^2/1944$. The radius of gyration of the ideal KS can easily be obtained from Eq. (20). In the limit $m \rightarrow \infty$, the area S_m tends to the area S^{KS} of the ideal KS, and $R_m \rightarrow R_{\text{KS}}$. Then by taking the limit from the both sides of Eq. (20) and cancelling S^{KS} from the numerator and denominator, we arrive at the linear equation for R_{KS}^2 , which yields $R_{\text{KS}}^2 = 4a^2/33$, and, hence, $R_{\text{KS}} = 2a/\sqrt{33}$. The scattering intensities are shown in Fig. 5. Generally, all the properties of the scattering curves are the same as in the case of Cantor-like surface fractals, presented above in Sec. III B. Since the overall size of KS is of order of a , the upper border of the Guinier range is about $2\pi/a$. The Fractal range lies between $2\pi/(a\beta_s)$ and $2\pi/(a\beta_s^{m+1})$, because the edge of smallest triangles equals $a\beta_s^{m+1}$.

Let us consider the contribution of different mass fractal amplitudes to the total scattering intensity of KS. Because of additivity of the scattering amplitude, each mass fractal amplitude can be calculated as the difference between amplitudes of two consecutive iterations of KS (see Fig. 3)

$$M_m(q) = A_{m-1}(q) - A_{m-2}(q), \quad (21)$$

where $m = 2, 3, \dots$. The zeroth mass fractal iteration is the largest triangle in Fig. 3, so we have $M_0(q) = A^T(q) = S^T F^T(q)$, and the first mass fractal amplitude is given by $M_1(q) = A_0(q) - A^T(q)$.

Inversely, one can write the KS amplitude as a sum of the mass fractal amplitudes

$$A_m(q) = \sum_{n=0}^{m+1} M_n(q). \quad (22)$$

Then the KS intensity $I_m(q) = \langle |A_m(q)|^2 \rangle$ contains not only the mass fractal intensities $\langle |M_n(q)|^2 \rangle$ but the correlations between the mass fractal amplitudes

$$I_m(q) = \sum_{n=0}^{m+1} \langle |M_n(q)|^2 \rangle + \sum_{0 \leq n < p \leq m+1} \langle M_n^*(q) M_p(q) + M_n(q) M_p^*(q) \rangle. \quad (23)$$

One can neglect the non-diagonal (interference) terms in this equation and even more, completely neglect the interference between the amplitudes of triangles composing the mass fractals. This approximations work well frequently, say, for the Cantor surface fractal (see Sec. III B above). However, this scheme does not work properly for the KS, see Fig. 6. The reason is that distances between different mass fractal iterations and between triangles within one mass fractal iteration

can be of order of their sizes, and we have to take into account the interference terms in Eq. (23).

Nevertheless, one can reduce the problem, in effect, to the incoherent sum of the “combined” mass fractals. Indeed, considering the correlations between two consecutive mass fractal iterations like $\langle M_0^* M_1 \rangle$, $\langle M_1^* M_2 \rangle$, and so on, and neglecting the other correlations, we obtain from Eq. (23)

$$I_m(q) \simeq \sum_{n=0}^m \langle |M_n(q) + M_{n+1}(q)|^2 \rangle - \sum_{n=1}^m \langle |M_n(q)|^2 \rangle \quad (24)$$

SAS from the surface Cantor fractal is described well by incoherent sum of *single* mass fractal intensities, while the first sum in the approximation (24) is nothing else but *incoherent sum* of intensities of *pairs* of consecutive amplitudes. The SAS intensities of each pair behave like a mass fractal with the power-law decay $I(q) \sim q^{-D_m}$ at $D_m = D_s$, which results in the power-law decay of the intensity (24) $I(q) \sim q^{D_s-2d}$ with $d = 2$ for the plane.

By analogy with the pair consecutive amplitudes, one can further improve the approximation (24) for the SAS intensity by including the triple consecutive amplitudes $\langle |M_n + M_{n+1} + M_{n+2}|^2 \rangle$. The results for the KS is shown in Fig. 6a.

One of the main properties is the approximate log-periodicity of the curve $I(q)q^{4-D_s}$ within the fractal range, which is illustrated in Fig. 6b. As one can see, complete ignorance of correlations between the mass fractal amplitudes leads to a bad approximation.

V. CONCLUSIONS

We have derived analytical expressions for the monodisperse form factor of 2D Cantor-like and Koch snowflake surface fractals, and have shown that at a given iteration m , both surface fractal models can be represented as a sum of mass fractals at iterations from zero to m . This confirms that in general, *any surface fractal can be represented as a sum of mass fractals*. While the “rough structure” of SAS (including the borders of fractal region and the power exponent $D_s - 6$) is determined by the power-law distribution of the triangle sizes, the superimposed interference structure of the intensity needs more precise approximations.

It is shown that for Cantor-like surface fractals, the correlations between mass fractal amplitudes can be neglected, however for the Koch snowflake the correlations between amplitudes are important, although they can be built in our model without changing the main conclusions. The log-periodicity of the curve $I(q)q^{4-D_s}$, where $1 < D_s < 2$, arises from the self-similarity of *sizes* of basic structural units, in contrast with mass fractals, where the log-periodicity arises from the self-similarity of *distances* between structural units.

The present analysis allows us to extract additional information from SAS data, such as the edges of the fractal region, the fractal iteration number and the scaling factor, as for the case of mass fractals.

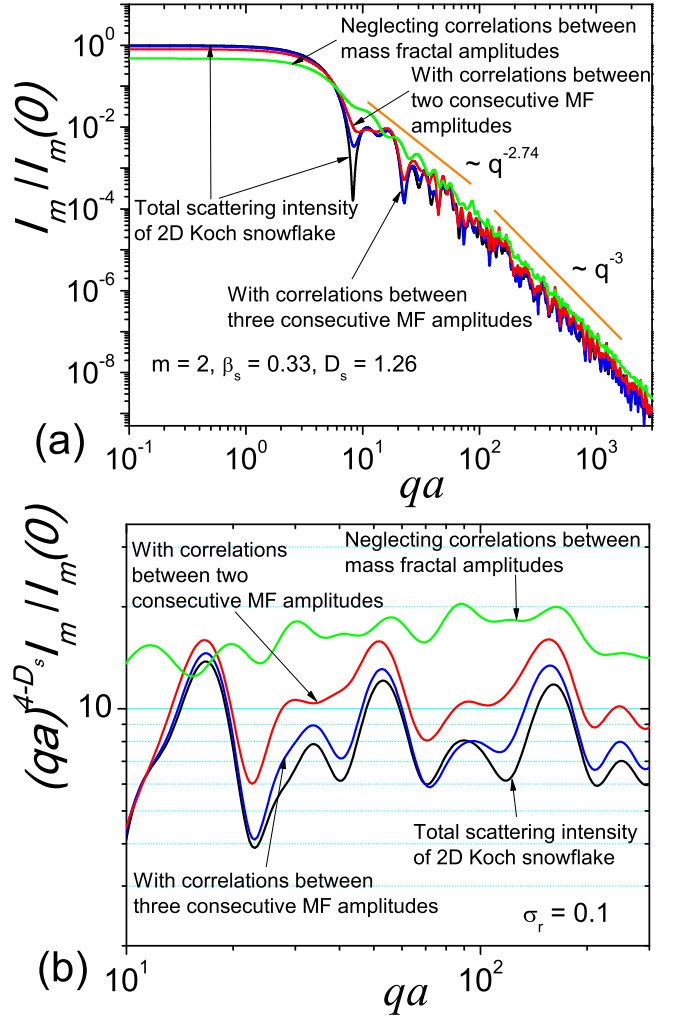


FIG. 6. (Color online) SAS from KS and its approximations by the scattering from the mass fractal composing KS (see Fig. 3). (a) The total intensity (black) and the intensities taking into account various correlations between the mass fractal amplitudes. The correlations between *three* consecutive mass fractal amplitudes are included (blue), and the same for the correlations between *two* consecutive mass fractal amplitudes (red). Neglecting all the correlations between mass fractals (green) is not good enough for describing the total intensity of KS. (b) Approximate log-periodicity of the curve $I(q)q^{4-D_s}$ with the period $\beta_s = 1/3$. The polydisperse scattering intensities are shown for the relative variance $\sigma_r = 0.1$. One can observe an interference between different mass fractal amplitudes, so their correlations are important.

ACKNOWLEDGMENTS

The authors acknowledge financial support from JINR–IFIN-HH projects. A.I.K. acknowledges Russian program “5Top100” of the Ministry of Education and Science of the Russian Federation.

Appendix A: Scattering from a triangle, hexagon and DS

Consider an isosceles triangle with the altitude h and the length of its base a . The area of triangle is equal to $S^T = ah/2$. We choose the Cartesian coordinate system where the base is parallel to the x -axes and the opposite vertex coincides with the origin. Then the normalized scattering amplitude is obtained with Eq. (4), which becomes now a surface integral

$$F^T(\mathbf{q}) = \frac{1}{S^T} \int_0^a dy \int_{-\frac{y}{2h}}^{\frac{y}{2h}} dx e^{-i(xq_x + yq_y)} \quad (\text{A1})$$

with the scattering vector $\mathbf{q} = \{q_x, q_y\}$. By calculating the integral, we arrive at the analytical expression

$$F^T(\mathbf{q}) = \frac{2e^{-i\alpha} (\beta e^{i\alpha} - \beta \cos \beta - i\alpha \sin \beta)}{\beta (\beta^2 - \alpha^2)}, \quad (\text{A2})$$

where we put by definition $\alpha \equiv hq_y$, $\beta \equiv aq_x/2$. For an equilateral triangle, we have $h = a\sqrt{3}/2$.

The scattering amplitude of any geometrical set, composed of triangles, can be obtained by summing the triangle amplitudes, which are appropriately scaled, rotated, and translated, see Sec. II. Then a hexagon can be constructed from the six equilateral triangles, and a star of David can be composed of one big equilateral triangle and three similar triangles scaled with the factor one third, see Fig. 3. The formulas for their scattering amplitudes are obvious, and we do not write them down explicitly.

Note that hexagon and star of David have the inversion symmetry $\mathbf{r} \rightarrow -\mathbf{r}$ with respect to their center-of-masses, and, thus, their amplitudes are real $A^*(\mathbf{q}) = A(\mathbf{q})$, provided the coordinate origin is chosen in the centers.

-
- [1] A. Guinier and G. Fournet, *Small-Angle Scattering of X-Rays* (John Wiley & Sons, Inc., New York, 1955).
 - [2] L. A. Feigin and D. I. Svergun, *Structure Analysis by Small-Angle X-Ray and Neutron Scattering* (Plenum, New York, 1987).
 - [3] H. Brumberger, *Modern Aspects of Small-Angle Scattering* (Kluwer Academic Publishers, Dordrecht, 1995).
 - [4] P. Lindner and T. Zemb, *Neutrons, X-Rays and Light: Scattering Methods Applied to Soft Condensed Matter* (Elsevier, Amsterdam, 2002).
 - [5] H. D. Bale and P. W. Schmidt, Phys. Rev. Lett **53**, 596 (1984).
 - [6] J. E. Martin and A. J. Hurd, J. Appl. Cryst **20**, 61 (1987).
 - [7] J. Teixeira, J. Appl. Cryst. **21**, 781 (1988).
 - [8] P. W. Schmidt, J. Appl. Cryst. **24**, 414 (1991).
 - [9] G. Beaucage, J. Appl. Cryst. **29**, 134 (1996).
 - [10] A. Yu. Cherny, E. M. Anitas, A. I. Kuklin, M. Balasoiu, and V. A. Osipov, J. Appl. Cryst. **43**, 790 (2010).
 - [11] A. Yu. Cherny, E. M. Anitas, V. A. Osipov, and A. I. Kuklin, Phys. Rev. E **84**, 036203 (2011).
 - [12] B. B. Mandelbrot, *The Fractal Geometry of Nature* (W. H. Freeman, 1983).
 - [13] J. F. Gouyet, *Physics and Fractal Structures* (Springer, 1996).
 - [14] E. M. Anitas, Eur. Phys. J. B **87**, 139 (2014).
 - [15] A. Yu. Cherny, E. M. Anitas, V. A. Osipov, and A. I. Kuklin, J. Appl. Cryst. **47**, 198 (2014).
 - [16] A. Yu. Cherny, E. M. Anitas, V. A. Osipov, and A. I. Kuklin, (2016), arXiv:1507.07376v2.
 - [17] G. R. Newkome, P. Wang, C. N. Moorefield, T. J. Cho, P. P. Mohapatra, S. Li, S. H. Hwang, O. Lukoyanova, L. Echegoyen, J. A. Palagallo, V. Iancu, and S. W. Hla, Science **312**, 1782 (2006).
 - [18] E. J. W. Berenschot, H. V. Jansen, and N. R. Tas, J. Micromech. Microeng. **23**, 055024 (2013).
 - [19] A. Rogachev, A. Cherny, A. Ozerin, V. Gordeliy, and A. Kuklin, Crystallogr. Rep. **52**, 500 (2007).
 - [20] A. Yu. Cherny, E. M. Anitas, V. A. Osipov, and A. I. Kuklin, Rom. J. Phys. **60**, 658 (2015).
 - [21] A. Burns, Math. Gazette **78**, 193 (1994).